Check for updates

RESEARCH ARTICLE

Design of a direct-drive axle-mounted traction motor for boosting high-speed trains

[version 1; peer review: awaiting peer review]

Jonan Morales Ramiro[1,2], Marco Satrústegui[1,2], Eneko Landa Ansa[1,2], Eduardo de la Guerra Ochoa[3], Miguel Martínez-Iturralde[1,2]

[1]ECAE, CEIT-Basque Research and Technology Alliance (BRTA), Manuel Lardizabal 15, 20018 Donostia/San Sebastián, Spain
[2]Departamento de Ingeniería Eléctrica y Electrónica, Universidad de Navarra - Campus San Sebastian, San Sebastián, Basque Country, 20018, Spain
[3]Talgo, Las Matas, Madrid, 28290, Spain

v1 **First published:** 17 Oct 2026, **6**:428
https://doi.org/10.12688/openreseurope.25316.1
Latest published: 17 Oct 2026, **6**:428
https://doi.org/10.12688/openreseurope.25316.1

Abstract

Background

High-speed railway traction systems must combine high efficiency and power density within constrained mechanical envelopes. This work presents the design and numerical assessment of a direct-drive permanent magnet synchronous motor (PMSM) for supplementary traction, designed to fit between the wheel and axlebox of an existing high-speed train while retaining its disc-brake hardware.

Methods

The design methodology combines multiobjective parametric optimisation with topology optimisation to limit magnetic flux leakage while preserving manufacturability. An oil-flooded, slot-through cooling system was integrated into the motor. Electromagnetic, thermal and structural simulations assessed nominal operation, fault conditions, overspeed, shock and vibration loads derived from railway standards. High-speed-boost and load-sharing strategies were benchmarked over a representative duty cycle against the reference geared induction-motor powertrain.

Results

This direct-drive architecture eliminates the gearbox and dedicated motor bearings. In the preliminary comparison based on estimated

Open Peer Review

Approval Status *AWAITING PEER REVIEW*

Any reports and responses or comments on the article can be found at the end of the article.

active-part masses, direct oil cooling enables approximately four times the power density of water-jacket cooling within the same envelope. Simulations predict 275 kW of continuous power and 95.54% nominal efficiency at 2275 rpm, corresponding to 360 km/h. The calculated assembly mass is 86.90 kg, including cooling oil, yielding 3.16 kW/kg. The motor achieves an envelope-based power density of 8.23 kW/L while retaining the existing disc-brake hardware. Duty-cycle simulations predict reductions of up to 5.82% in electricity-related operating costs and emissions with load sharing.

Conclusions

The results support the numerical feasibility of a compact, high-power-density direct-drive motor for supplementary railway traction. The proposed architecture integrates direct oil cooling and axle-mounted mechanical design while retaining the existing brakes, providing the basis for prototype manufacture and experimental validation in subsequent work.

Plain Language summary

High-speed trains can use additional motors to improve acceleration, but conventional traction systems require gearboxes and other mechanical components that add weight and energy losses. This study develops a compact electric motor designed to be retrofitted between the wheel and axlebox without removing or modifying the existing disc-brake hardware. Its rotating part is mounted directly on the axle, while the housing is attached to the axlebox, eliminating the need for a gearbox and additional motor bearings. Oil flows through the motor to remove heat. Computer simulations assess its performance during normal operation, electrical faults, excessive speed, vibration and shock. The final motor has a calculated mass of 86.90 kg, including cooling oil, and simulations predict a continuous output of 275 kW with an efficiency of 95.54%. When the added motor shares the traction demand with the existing induction motors over the modelled journey, electricity-related operating costs and associated carbon dioxide emissions could fall by up to 5.82%. These findings demonstrate the potential of the concept; prototype manufacture and testing are planned to confirm the simulated performance.

Keywords

Railway Traction, Distributed Traction, Direct Drive Motor, In-Wheel Motor, Axle-Mounted Motor

HE This article is included in the Horizon Europe gateway.

Corresponding author: Jonan Morales Ramiro (jmoralesr@ceit.es)

Author roles: Morales Ramiro J: Conceptualization, Data Curation, Formal Analysis, Investigation, Methodology, Software, Validation, Visualization, Writing – Original Draft Preparation; **Satrústegui M**: Funding Acquisition, Project Administration, Resources, Software, Supervision, Validation, Writing – Review & Editing; **Landa Ansa E**: Methodology, Resources, Validation, Writing – Review & Editing; **de la Guerra Ochoa E**: Conceptualization, Project Administration, Resources, Writing – Review & Editing; **Martínez-Iturralde M**: Funding Acquisition, Project Administration, Resources, Supervision, Writing – Review & Editing

Competing interests: The authors are employed by CEIT and Talgo as indicated in their affiliations. This work is related to the patent application cited in reference [35].

Grant information: This project has received funding from the European Union's Horizon Europe research and innovation programme under Grant Agreement No. 101101917 (FP4 - Rail4EARTH, Europe's Rail Flagship Project 4 - Sustainable and Green Rail Systems).
The funders had no role in study design, data collection and analysis, decision to publish, or preparation of the manuscript.

Copyright: © 2026 Morales Ramiro J *et al*. This is an open access article distributed under the terms of the Creative Commons Attribution License, which permits unrestricted use, distribution, and reproduction in any medium, provided the original work is properly cited.

How to cite this article: Morales Ramiro J, Satrústegui M, Landa Ansa E *et al.* **Design of a direct-drive axle-mounted traction motor for boosting high-speed trains [version 1; peer review: awaiting peer review]** Open Research Europe 2026, **6**:428 https://doi.org/10.12688/openreseurope.25316.1

First published: 17 Oct 2026, **6**:428 https://doi.org/10.12688/openreseurope.25316.1

1. Introduction

The railway sector plays a crucial role in modern transportation systems, providing an efficient and sustainable means of transporting passengers and freight. As the demand for higher speeds, improved efficiency, and reduced environmental impact continues to grow, advancements in railway traction technologies have become increasingly important.[1]

A promising area of research is the development of distributed traction solutions for railway applications, which involve integrating multiple motors into various axles to evenly distribute tractive effort throughout the train. This approach offers several advantages, including enhanced acceleration, improved weight distribution, and increased braking efficiency.[2] Additionally, distributed traction systems enable trains to operate smoothly under varying track conditions, thereby improving overall control and performance. Some manufacturers are introducing these technologies in recent models.[3–7]

A significant advancement in distributed propulsion is the integration of direct-drive motors, which eliminate the need for transmission components such as gearboxes by coupling the rotor directly to the axle. This configuration enhances drivetrain efficiency by reducing mechanical losses and system weight, while also providing smoother operation and lower maintenance requirements. Directly connecting the motor to the axle simplifies the drivetrain, increasing its durability and reliability, which is particularly well-suited to the demands of modern high-speed trains.[8,9] Nevertheless, the mechanical integration of the motor is complex due to space constraints, particularly in existing bogie designs, requiring precise engineering to ensure the motor can be fitted without compromising the system's structural integrity or performance. Additionally, being directly coupled to the axle, the motor must endure shocks and vibrations without the cushioning effect of suspension systems, which can lead to bearing faults, necessitating a more robust mechanical design to operate reliably under such aggressive conditions.[10–12]

Permanent magnet synchronous motors (PMSMs) emerge as an ideal solution for direct-drive railway applications, offering significant advantages over traditional induction motors. These advantages include higher efficiency (from 91%-92% to 94%-96%), particularly during partial-load operation, which is common in railway systems.[13] Additionally, PMSMs provide greater torque density, enabling more compact and lightweight designs—a critical factor for axle-mounted configurations where space is limited.[14–16] Furthermore, PMSMs exhibit superior dynamic performance, with faster response times and better controllability, making them particularly suitable for high-speed and high-performance railway applications.[17] However, the transition to PMSMs entails higher control-hardware costs due to the requirement of a dedicated inverter for each motor, unlike induction motors, which can often be grouped under a single drive. These life-cycle energy savings and spatial benefits position PMSMs as a transformative technology for modern railway traction systems.

Given the brittle nature of sintered magnets—commonly used for their high energy density—particular attention must be paid to their mechanical integrity under dynamic loading. These materials exhibit low fracture toughness and are especially sensitive to tensile and shear stresses perpendicular to their preferred magnetisation axis, often leading to intergranular failure.[18–22] In demanding environments such as axle-mounted railway applications, where shock, vibration, and thermal gradients coexist, ensuring the structural stability and secure retention of these magnets becomes a key design constraint. Therefore, special emphasis is placed in this work on evaluating magnet behaviour and fixation strategies to mitigate mechanical degradation and demagnetisation risks during operation.

However, the high power density and compact design of axle-mounted motors pose significant thermal management challenges. Conventional cooling methods, such as air cooling or indirect water-jacket systems, often prove inadequate in these confined environments. In contrast, direct oil cooling provides efficient heat absorption and dissipation without introducing excessive mechanical complexity or weight, making it especially suitable for the demanding operating conditions of railway applications.[23–25]

The PINTA3/MK5 demonstrator provides a relevant comparison for direct-drive traction in high-speed trains, addressing the same application through an integration approach that involved modifications to existing running-gear components and omitted the wheel-mounted brake discs.[26,27] Developed within Europe's Rail Flagship Project 4 (FP4) Rail4EARTH, the present study addresses a distinct set of integration requirements: providing supplementary traction within the available wheel-to-axlebox envelope while retaining the existing disc-brake hardware. The distinguishing contribution is a high-power-density axle-mounted PMSM design that meets these packaging objectives through a compact motor and mounting architecture requiring no dedicated motor bearings. The design combines parametric and topology optimisation with direct oil cooling to support the required continuous power within the constrained envelope, maximising power density. A central aspect of this contribution is the integration of the cooling circuit, oil routing and sealing arrangement with the mechanical design to address both heat removal and oil containment under the shocks and vibrations associated with direct axle mounting. Electromagnetic, thermal and structural simulations assess the design under the specified

operating, fault and mechanical load cases, while duty-cycle benchmarking quantifies its operational implications relative to the reference geared induction-motor powertrain. The scope is design and numerical assessment; prototype-level experimental validation is reserved for a subsequent study.

The remainder of the paper is organised as follows. Section 2 defines the case-study requirements, describes the motor-design process from multiobjective parametric optimisation through topology refinement, and reports the electromagnetic and thermal simulation results. Section 3 presents the mechanical integration of the motor into the bogie, including the direct-drive layout and the cooling and sealing arrangements, and assesses the design under static, overspeed, shock, and vibration load cases derived from the relevant railway standards. Section 4 compares the reference, high-speed-boost, and load-sharing traction configurations over the adopted duty cycle and reports their cycle-efficiency, modelled operating-cost, and carbon-emission estimates; it also compares the proposed design with the PINTA3/MK5 demonstrator in Section 4.2. Section 5 summarises the main numerical findings and identifies prototype manufacture and experimental testing as the next stage of the work.

2. Case study and design methodology

This research explores a specific case study provided by Talgo,[28] developing a supplementary traction system for the Talgo Avril G3 high-speed train.[29] The goal is to design a PMSM-based direct-drive motor prototype that enhances acceleration capabilities at high speeds, ranging from 150 to 360 km/h, in order to increase the efficiency and power density of the powertrain and reduce related CO_2 emissions.

The use case requires a set of motors providing an additional tractive effort of 27 kN, as shown in Figure 1.

To provide the required traction capacity, the PMSMs shall be distributed across various axles throughout the train. They will be installed in the available space between the wheel and the axlebox, without modifying the disc-brake system of each wheel to preserve the train's braking capability. This strategic placement allows for efficient power distribution while adhering to spatial constraints and safety requirements. Table 1 outlines the specific dimensional and performance requirements of the application.

The design methodology adopted in this work is structured into three main stages: predesign, topology optimisation and multiphysics validation through finite element method (FEM) and computational fluid dynamics (CFD) simulations.

2.1 Predesign

The initial design was governed by a multiobjective parametric optimisation process called multiobjective differential evolution (MODE)[30] that iteratively refined the coupled electromagnetic, thermal, and mechanical constraints. This predesign stage focused on identifying the most efficient and robust motor architectures by defining and thoroughly comparing several candidate configurations through hybrid analytical-FEM simulations. Specific design variables, including pole-slot combinations, interior permanent magnet (IPM) topologies and different water and oil cooling

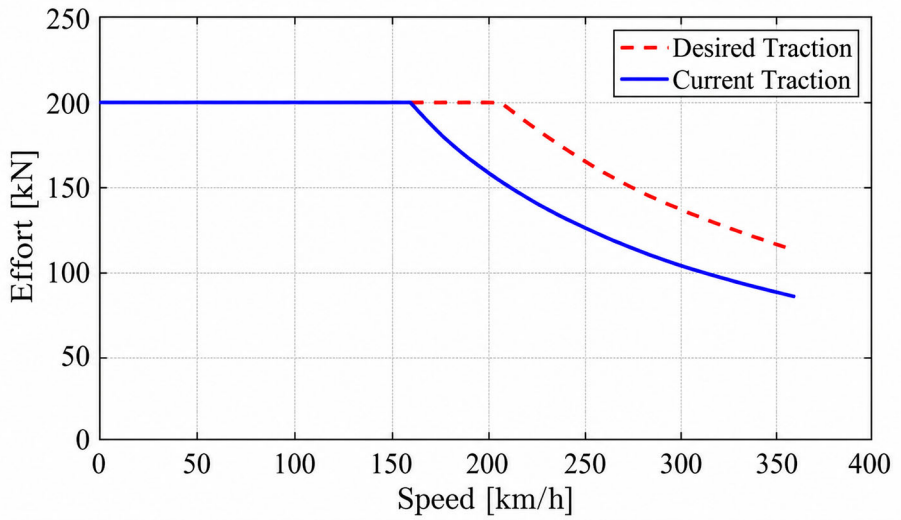


Figure 1. Comparison between current traction and desired traction.

Table 1. Main requirements for the designated motor.

Parameter	Requirement
Number of motors	*16*
Envelope [mm]	*230 × Ø430*
Power [kW]	*275*
Torque [N m]	*1155*
Whole motor power density [kW/kg]	*>1*
Operating speed [rpm]	*1260–2275*

Table 2. Initial motor configuration for the parametric design study.

Parameter	Initial configuration
Cooling arrangement	Liquid cooling
Winding type	Concentrated wire winding
Rotor topology	Interior permanent magnets
Stator slots	36
Pole pairs	12
Stator outer diameter [mm]	380
Active stack length [mm]	100
Physical air gap [mm]	1.5

arrangements, were input into the parametric optimisation algorithm. This methodology ensured that each candidate was driven to its maximum performance potential, enabling a precise, quantitative comparison through three key performance indicators: motor efficiency, power density in active parts and the mass of the permanent magnet material.

To establish the optimal motor configuration, a radial-flux IPM configuration was adopted as the starting point for the parametric design study. A concentrated wire winding was selected to minimise the axial space occupied by the end-windings, thereby maximising the active stack length within the available installation envelope. The initial configuration comprised 36 stator slots and 12 pole pairs. This combination was selected based on previous design experience concerning power density and harmonic behaviour, with a high pole count pursued to support the required torque density. This choice also motivated the consideration of a spoke-type rotor, which offered the possibility of accommodating a larger permanent-magnet volume within the selected pole arrangement.

Table 2 summarises the initial configuration used to start the parametric study. These parameters describe the starting design rather than the final optimised geometry.

Meeting the strict 275 kW continuous power requirement within the available spatial envelope required a rigorous comparative analysis of thermal management strategies and rotor designs. Figure 2 illustrates the candidates for water-jacket cooling and oil-flooded direct cooling across V-shaped and spoke-type IPM topologies. The cooling comparison used corresponding motor designs within the same installation envelope. The water-jacket variant required no internal oil-sealing component and allowed a smaller air gap and a higher slot fill factor. Apart from these cooling-dependent changes, the remaining components and geometry were retained. The comparison therefore evaluates the maximum continuous performance of the two cooling arrangements under the adopted design constraints. At this preliminary design stage, active-part masses were estimated for each candidate and used to calculate the corresponding power densities; these estimates are approximate and therefore differ from those reported in the mass breakdown of the final detailed design (with the final active-part mass 10% lower than estimated). As demonstrated by the results, the water-jacket system is thermally limited to a continuous output of 66 kW (0.94 kW/kg in active parts). In contrast, the oil-flooded approach successfully achieves the 275 kW target (3.97 kW/kg in active parts) by overcoming severe volumetric constraints. Based on these performance disparities, the oil-flooded spoke-type IPM was identified as the most suitable architecture. The final design was ultimately selected from its corresponding Pareto set by integrating a life-cycle energy consumption

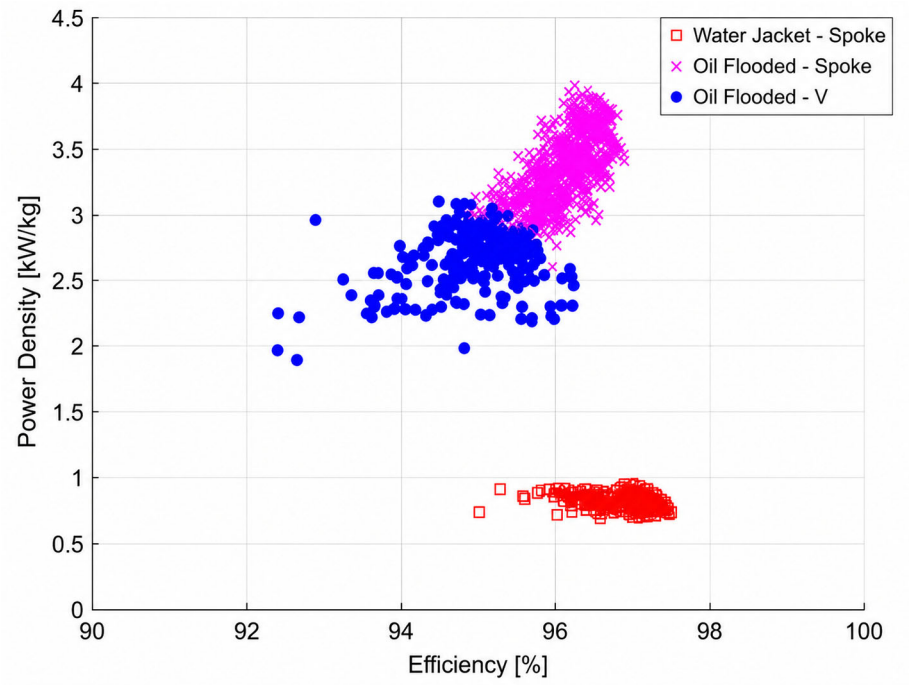


Figure 2. Comparison of different rotor topologies and cooling systems in terms of power density and efficiency.

analysis based on the EN 50591[31] standard. The analysis indicated that a magnet-optimised configuration maximising high-speed efficiency offers the lowest overall operational cost despite higher initial material investments.

2.2 Topology optimisation

Once the rotor geometry was selected through parametric optimisation, a topology optimisation stage was performed using the density method and the level-set method[32] coupled with finite element analysis[33] to refine the design from both electromagnetic and mechanical perspectives. This method identified regions with limited electromagnetic contribution and reduced their material density, as shown in Figure 3, particularly around the structural bridges in spoke-type IPM configurations, where material could be strategically removed to reduce flux leakage and enhance torque production without compromising mechanical integrity. The results served as a valuable guideline for subsequent manual redesign, enabling an improved balance between manufacturability, mechanical robustness, and electromagnetic efficiency.

In an ideal scenario, disregarding mechanical constraints, the inner bridge should be completely eliminated to avoid creating a low-reluctance path for flux leakage, ensuring it passes solely through air or non-ferromagnetic materials. However, this represents a non-manufacturable theoretical limit. To ensure the manufacturing feasibility of the laminations, the manufacturer specified a minimum inner rotor bridge width of 5 mm. Directly implementing a solid bridge of this dimension without optimisation would result in excessive flux leakage, causing a significant reduction in the machine's output torque. The voids incorporated using topology optimisation as a guide (see Figure 4) effectively mitigate this leakage, yielding a 15.7% increase in torque compared to the non-optimised design under identical supply conditions.

2.3 Multiphysics simulation of active parts

A comprehensive multiphysics analysis was conducted using FEM and CFD simulations to confirm the final design's robustness under both nominal and fault conditions. The electromagnetic analysis evaluated performance under pulse-width-modulation (PWM), using the calculated loss data to thermally validate the oil cooling system's capacity to maintain critical components within safe limits, while also ruling out demagnetisation risks during short-circuit events. Concurrently, the mechanical analysis verified the structural integrity of the rotor and stator against extreme stresses, ensuring they withstand overspeed conditions (+20%) and maximum short-circuit torque without compromising the machine's operation.

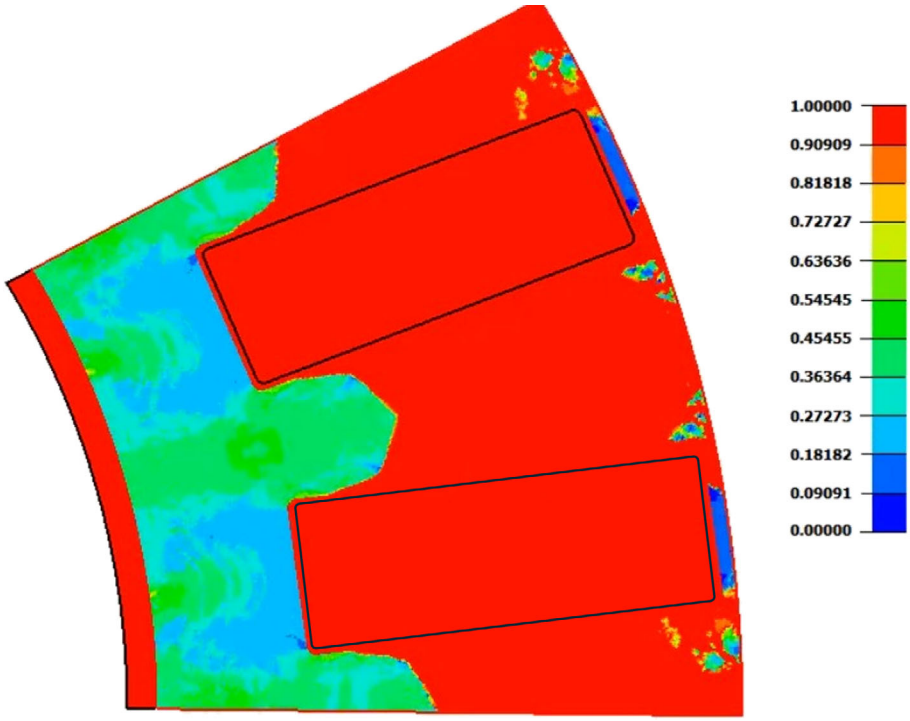


Figure 3. **Result of the topology optimisation applied to the selected spoke-type permanent magnet rotor.**

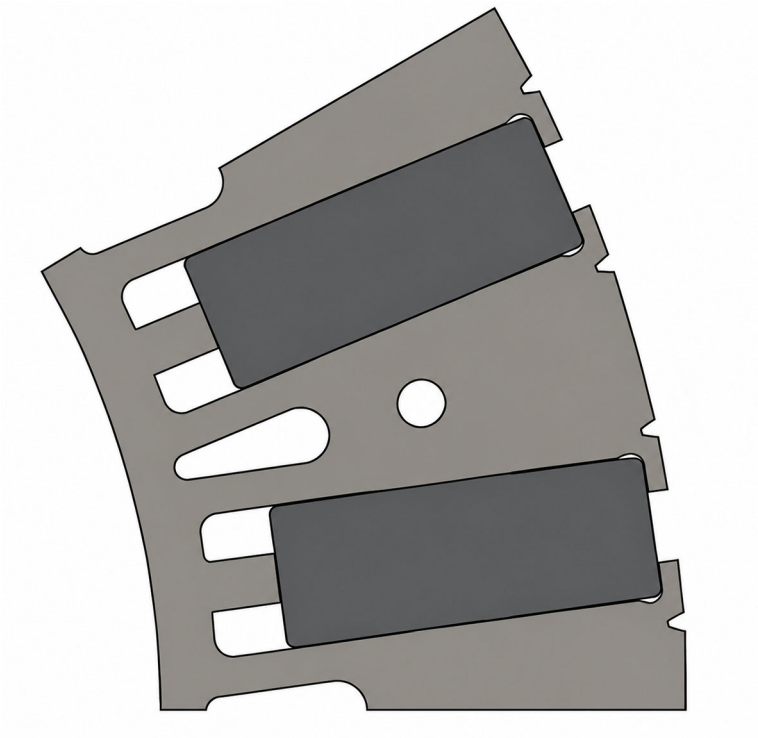


Figure 4. **Final rotor design after topology optimisation.**

Table 3. Performance of the machine.

Variable	Value
Rated speed [rpm]	*2275*
Rated power [kW]	*275*
Rated torque [N m]	*1154*
Efficiency [%]	*95.54*

2.3.1 Electromagnetic performance

FEM electromagnetic simulations were carried out using Altair Flux to validate electromagnetic performance. The results in Table 3 summarise the key performance characteristics under PWM excitation.

The summarised results confirm that the proposed motor design successfully meets the performance targets for the auxiliary traction application. Under nominal operating conditions, the machine delivers a rated power of 275 kW and a torque of 1154 N m at a rated speed of 2275 rpm. Notably, the design achieves a high nominal efficiency of 95.54%, validating the effectiveness of the proposed topology and cooling strategy in maximising energy conversion within the required spatial constraints. These loss estimates were performed assuming a non-segmented magnet configuration. Given the elevated levels of eddy current losses observed in the magnets under PWM operation, a conservative axial segmentation of 5 mm has been adopted. This design decision significantly reduces magnet heating and ensures margin with respect to the material's maximum operating temperature, thereby improving thermal reliability under inverter-fed operation.

Furthermore, the selected magnet grade and rotor topology have demonstrated strong resilience against fault-induced demagnetisation. Even under a conservative and highly stressful scenario—maximum speed, elevated temperature (160 °C), and direct three-phase short-circuit—the motor remains operational with minimal performance degradation, losing 3.58% of the rated torque in these extreme conditions. This reinforces the design's robustness and confirms its suitability for railway traction applications, where fault tolerance, thermal stability, and long-term reliability are critical.

2.3.2 Thermal results

The thermal analysis results presented below, obtained using CFD tools,[34] provide insight into the temperature distribution within the motor's active components during nominal operation. Particular attention was given to the winding and magnet temperatures, which represent the most thermally constrained areas of the machine.

The results show a uniform temperature distribution across the stator with no significant hotspot. The direct oil cooling approach effectively removes heat from the most thermally loaded areas, maintaining the winding average temperatures below the insulation class limit, with a hotspot just at the limit. In this case, a thermal class rated up to 200 °C would be required, as this corresponds to the hottest point within the winding. Additionally, the maximum temperature observed in the permanent magnets remains within the safe operating range, well below 180 °C, ensuring stable magnetic performance during continuous operation (see Table 4).

Table 4. Temperature distribution.

Variable	Value
Magnet average temperature [°C]	*130*
Magnet hotspot [°C]	*141*
Winding average temperature [°C]	*185*
Winding hotspot [°C]	*201*
Oil temperature gradient [°C]	*11.7*
Oil inlet temperature [°C]	*60*
Oil flow rate [L/min]	*40.0*

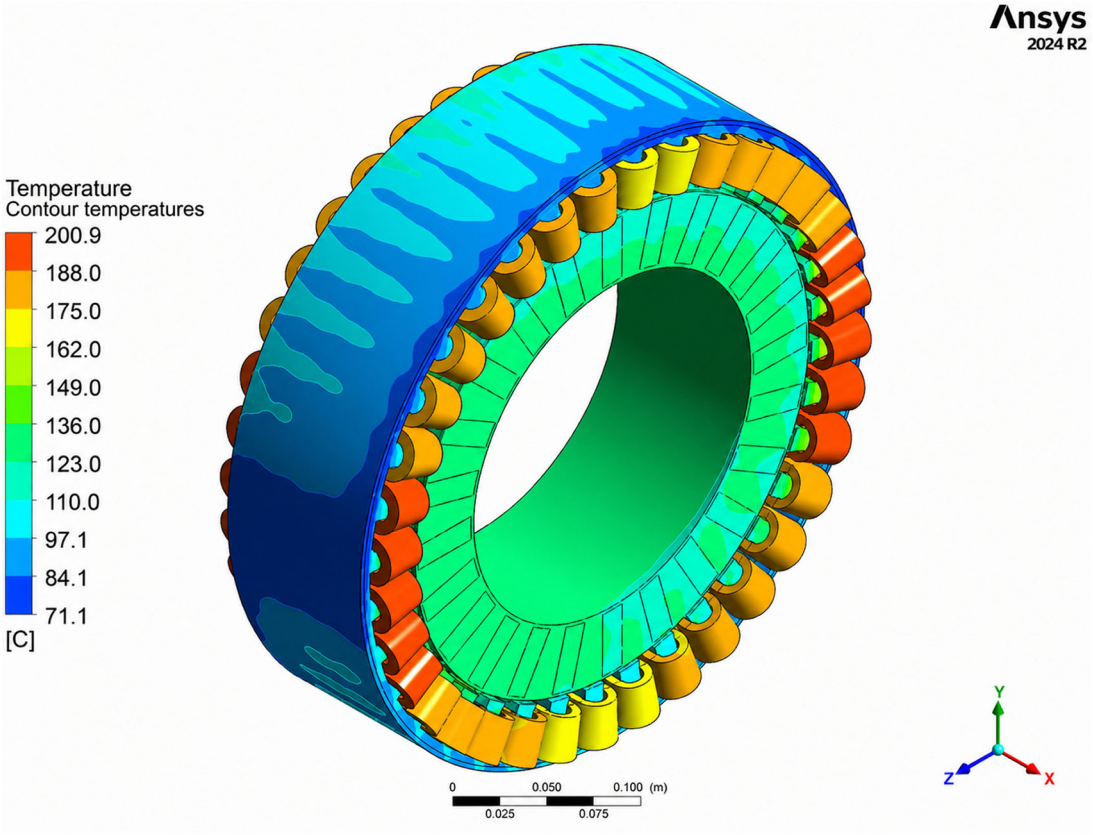


Figure 5. Temperature distribution across the active parts of the motor.

To complement these data, Figure 5 provides a detailed visualisation of the temperature distribution across the active parts of the motor.

3. Mechanical integration into the bogie

The developed motor follows a direct-drive architecture, in which the rotor is press-fitted directly onto the axle, enabling torque transmission without intermediate mechanical elements such as gearboxes, chains or belts. This solution[35] offers significant advantages in terms of compactness, mechanical simplicity, and maintenance reduction—key factors in railway applications. The press fit was sized using conventional interference-fit calculations to transmit the maximum torque considered in the design. The installation retains the existing disc-brake hardware without modification.

The motor housing has been shaped to match the available space envelope around the axle while ensuring mechanical rigidity and thermal performance. It is bolted in a cantilever arrangement with no dedicated motor bearings. Combined with the integrated oil-cooling system, this architecture enables high torque density within a tightly constrained volume. Figure 6 shows the general architecture of the motor assembly in the available space between the wheel and the axlebox.

3.1 Cooling system and sealing

The oil-flooded cooling system is integrated within the motor housing to remove heat from the active parts while accommodating the restricted wheel-to-axlebox installation envelope. The housing and internal containment ring define a confined oil circuit that floods the end-winding area and directs the coolant through the stator slots and towards the return duct through a sump. O-ring seals are incorporated at the interfaces between the containment ring, housing and endplates to contain the oil within the intended flow passages. Sealing provisions are also incorporated at the electrical connection interfaces.

The cooling circuit layout combines heat removal with the integration requirements associated with the exposed position of the axle-mounted motor beneath the vehicle. A dedicated return duct integrated into the housing also serves as a cooling jacket, contributing to stator heat removal while routing the oil towards the upper section of the motor (see

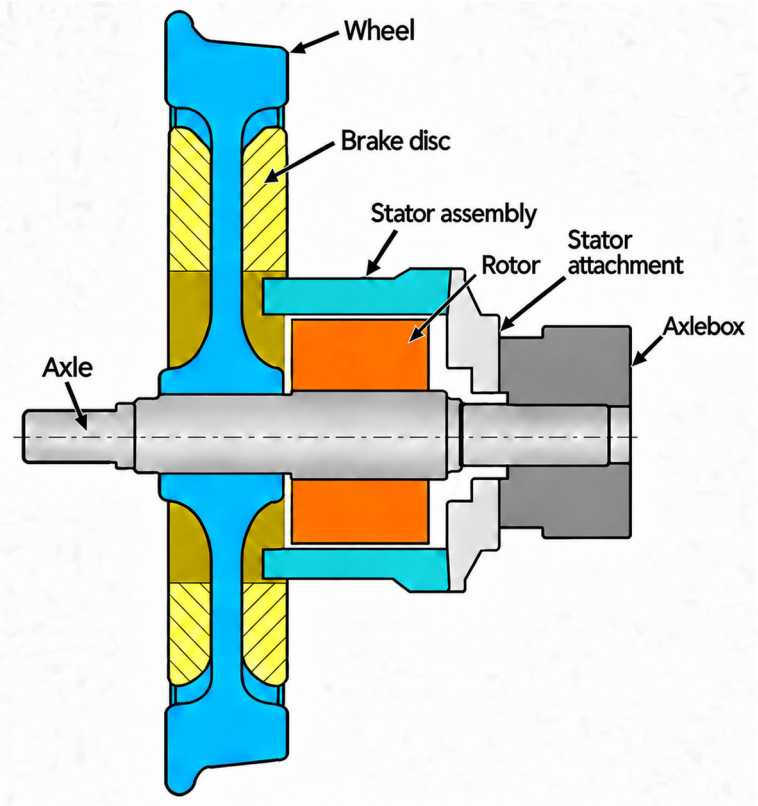


Figure 6. **General architecture of the motor assembly.**

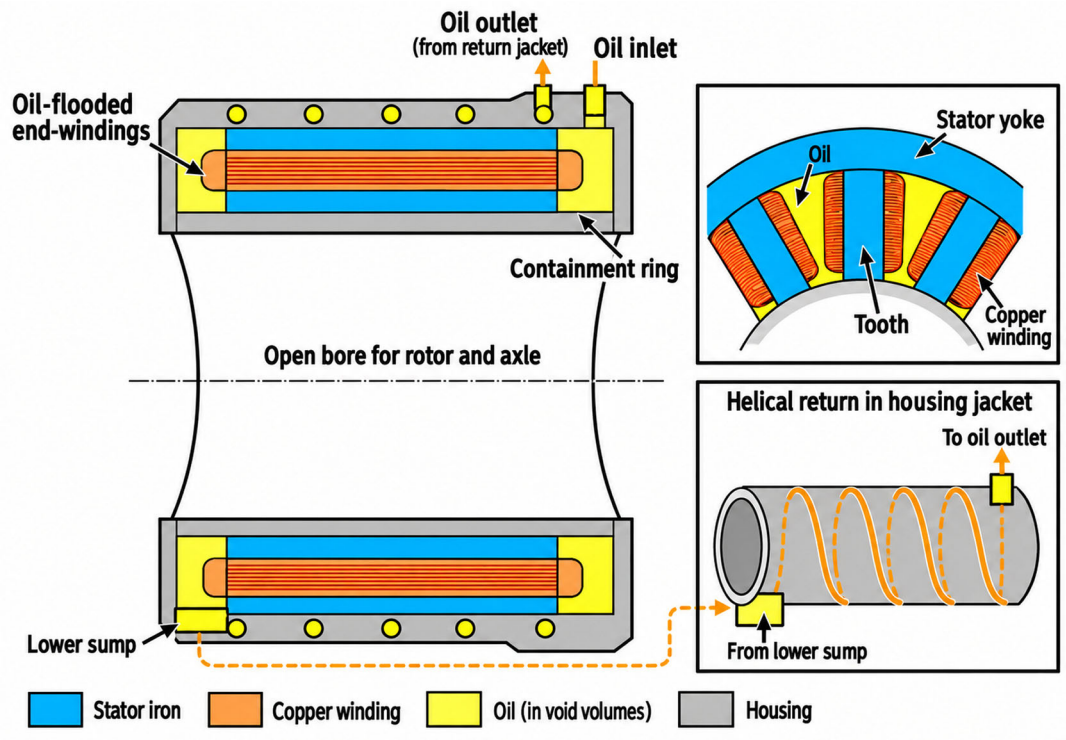


Figure 7. **Schematic of the cooling circuit.**

Figure 7). This arrangement reduces the exposure of the external return connection to ballast and debris and accommodates the coolant routing within the available mechanical envelope while limiting exposed pipework.

Figure 8 shows the principal components defining the cooling passages and sealing interfaces. Their integration is intended to maintain oil containment and the prescribed coolant flow path under the thermal and mechanical conditions of the application.

3.2 Railway standard compliance

In the context of direct-drive railway traction, mechanical integration is not limited to spatial packaging or fixation strategies—it must ensure that the entire motor assembly can withstand real-world operational loads, vibrations, and shocks throughout its service life. This becomes especially critical when the motor is axle-mounted, as both the rotor and stator are directly exposed to track-induced mechanical stresses. Therefore, compliance with relevant railway structural and vibrational standards is one of the most demanding aspects of mechanical integration and plays a key role in the overall reliability of the system.

To rigorously validate the motor design against these standards, a comprehensive finite element analysis (FEA) methodology was developed and implemented.[36] This robust approach was specifically tailored to evaluate the structural integrity of the system under both severe static and dynamic loading conditions. Independent, high-fidelity models were established for the stator and rotor assemblies to accurately capture their distinct structural behaviours.

To ensure a conservative and reliable assessment, the fixed components—including the stator, the housing, the cooling system and containment ring—were represented in their installed cantilever configuration.

Regarding the rotor, the analysis focused on the magnet retention system, which relies on adhesive bonding within the slots rather than an interference fit. To accurately capture this behaviour, two modelling approaches were employed: for static scenarios, the adhesive was simplified as a 0.1 mm-thick layer; for dynamic simulations, it was modelled with springs that represented the stiffness of this effective bonded area using the adhesive properties supplied by the manufacturer. Since there are no specific standards dictating the exact modelling parameters for adhesive in motor slots, a conservative heuristic approach was adopted based on the manufacturer's empirical know-how and extensive engineering experience. To account for the inherent variability in the adhesive application process, such as uneven distribution, void formation and long-term thermo-mechanical ageing, the effective bonding area was deliberately restricted to 30%. This assumption guarantees a conservative worst-case scenario for the structural assessment. It is important to note that the adhesive is treated as a secondary safety measure; the rotor slot geometry is designed to mechanically retain the magnets and withstand operational loads even in the event of adhesive failure, satisfying the requirement for dual retention mechanisms. Both assemblies were discretised using high-order tetrahedral elements with local mesh refinement applied to contact interfaces and stress concentration regions.

To establish a consistent and robust acceptance criterion across all evaluated load cases, distinct failure theories were applied depending on the nature of the materials. For ductile metallic components, such as the structural frame and rotor

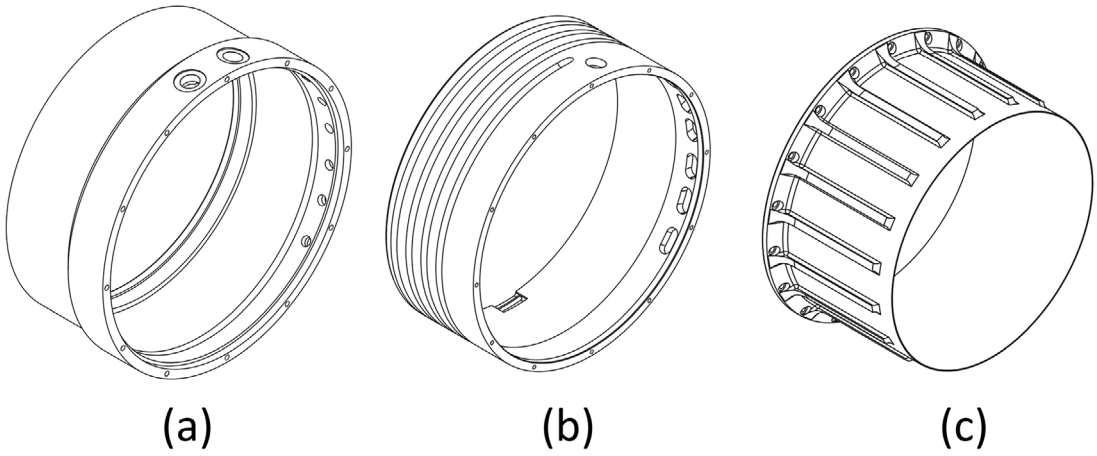


Figure 8. Components of the cooling and sealing system: (a) housing jacket, (b) housing body and (c) containment ring.

laminations, the von Mises equivalent stress criterion was employed, with the maximum allowable stress strictly limited to the material's yield strength to prevent any plastic deformation. Permanent magnets, however, are inherently brittle materials characterised by a significant disparity between their tensile and compressive strengths. Consequently, their structural integrity was assessed using the Mohr-Coulomb stress criterion for brittle materials[37] . This approach accurately captures the asymmetric failure behaviour of brittle materials, providing a highly reliable safety assessment of the magnetic poles under the severe conditions dictated by the railway standards.

3.2.1 Assessment under static structural load cases

To assess structural integrity under operational conditions, the motor assembly was evaluated using selected load cases derived from EN 13749:2011.[38] Given the rigid attachment of the motor housing to the axlebox, these load cases were adopted by analogy as a reference for the structural assessment. Static structural simulations were used to evaluate the assembly under the selected loads and load combinations. This assessment characterises the response to the adopted loading conditions and does not establish full compliance with the standard.

In the case of the stator and housing, the loads acting on the assembly are the maximum torque, self-weight and inertial loads due to the acceleration of the train. For this purpose, the maximum short-circuit torque was considered and applied to the stator slots, since it is the peak torque the motor must withstand instantaneously. The weight and inertial loads are especially relevant since the motor is fixed in a cantilever configuration, separating the centre of gravity from the fixed support and elevating the mechanical stress in the joints. In this analysis, controlling the maximum displacement at the cantilevered end is crucial to maintain the air gap clearance and avoid physical interference between the rotor and the containment ring of the cooling system. Due to the properties of the assembly, this simulation modelled the whole assembly without applying symmetry. The bolted joints inside the assembly were simplified and considered as bonded connections. However, special attention was given to the bolted joint between the housing and the axlebox, considering a pretension represented by a nominal axial stress of 430 MPa in the bolts according to the VDI 2230:2014 standard.[39]

The following results detail the stress and displacement levels observed in the structural parts of the motor under standard-defined operational loads, verifying the adequacy of the active components for axle-mounted integration. The maximum stress in the aluminium parts was found to be 90 MPa, with a maximum displacement of 0.04 mm, remaining well within the safety margins of 7075 aluminium alloy, whose yield strength is 460 MPa, providing a safety margin of 5.11 (see Figure 9). A local peak of 548 MPa was observed in the simulation at the contact area of the bolted interface. However,

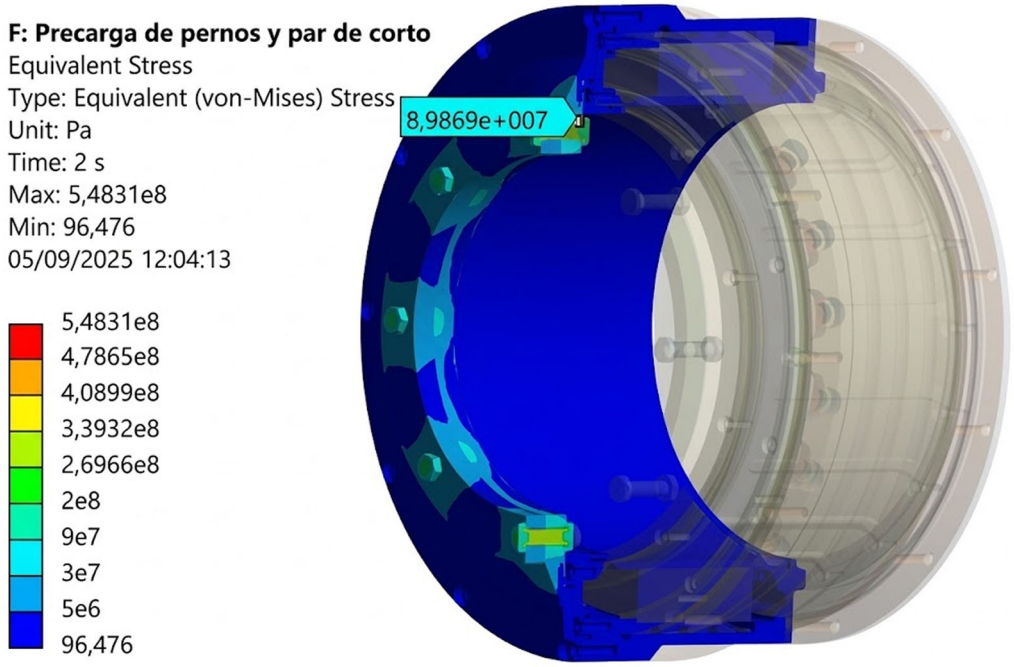


Figure 9. Equivalent von Mises stress map in the housing and flange under operational loads.

this is attributed to boundary conditions applied in the model where the axlebox was not explicitly included. Therefore, the concentration is not physically representative of the complete system and does not affect the validity of the stress evaluation in the motor's structural parts.

These results confirm the motor's structural adequacy for axle mounting, ensuring robustness against all defined operational loads while preserving alignment and air gap stability.

For the rotor, the same maximum torque was applied, but in this case the most critical load is the rotational speed. According to the railway electric traction standard EN 60349-2:2010,[40] the machine must withstand an overspeed of 20% above its maximum operating speed. Although the nominal maximum train speed for this application is 360 km/h (~2275 rpm), the specific use case requirements demand structural integrity up to 400 km/h (~2500 rpm). Therefore, a conservative approach was adopted by applying the margin to 2500 rpm and assessing the motor at 3000 rpm.

The results for the lamination confirm that the peak stress levels remain below the yield strength (359 MPa at 150 °C according to a previous in-house material test), providing an adequate safety margin (see Figure 10 and Table 5). Moreover, rotor deformation does not compromise air-gap stability or the mechanical retention of the magnets. For the magnets, the safety factor calculated using the Mohr-Coulomb criterion is even higher (see Figure 11 and Table 5). The stress levels remain well below the limit according to the diametral tensile stress for the most conservative scenarios reported in the literature.[18]

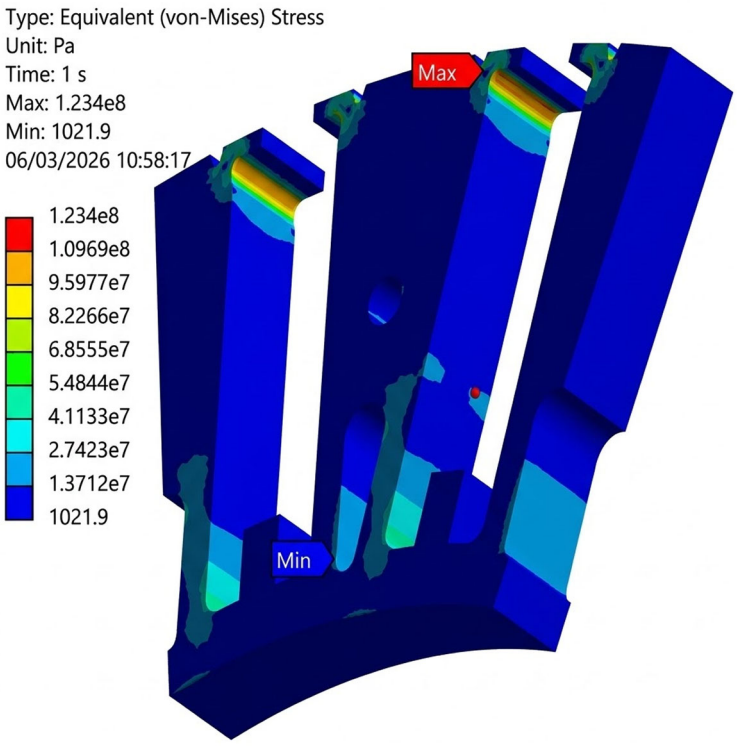


Figure 10. Equivalent von Mises stress map in the rotor for unglued magnets under operational loads.

Table 5. Safety factor for rotor components.

Component	Glued magnets	Unglued magnets
Rotor lamination	*6.59*	*2.91*
Permanent magnets	*8.87*	*7.90*

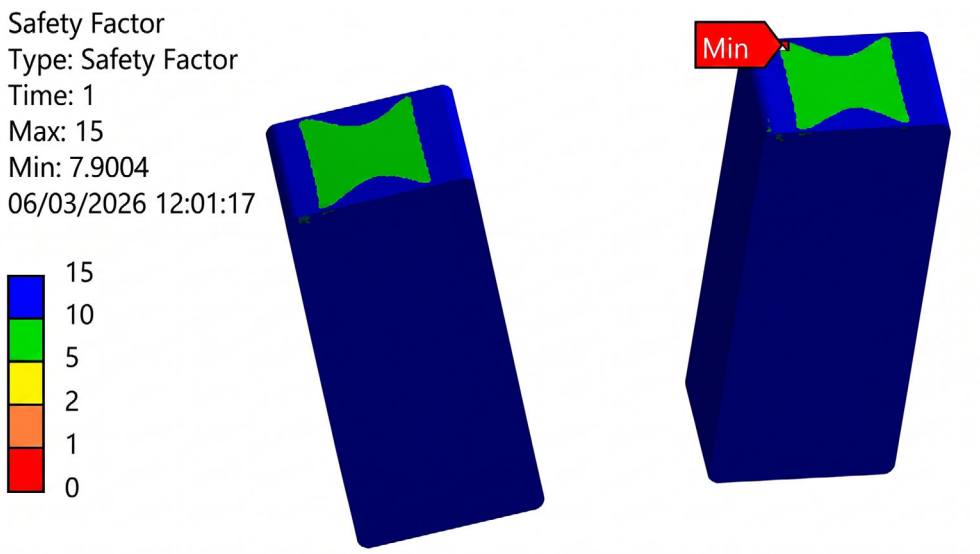


Figure 11. Safety factor according to the Mohr-Coulomb stress criterion for unglued magnets under operational loads.

This mechanical validation confirms that the active parts of the motor comply with the structural requirements of the application and show no plastic deformation. Both the rotor and stator demonstrate a mechanically sound response under nominal and extreme conditions, ensuring air gap stability and long-term operational reliability.

3.2.2 Assessment under dynamic load cases

To validate the motor's resistance to mechanical shocks and vibrations during railway operation, simulations have also been performed in accordance with EN 61373:2010,[41] which specifies the test requirements for vibration and mechanical shock in railway equipment. The motor was evaluated under Category 3 (Axle-Mounted Equipment), the most demanding profile defined by the standard. Prior to the spectral analysis, a modal extraction was performed to characterise the dynamic stiffness of the assemblies. Natural frequencies and mode shapes were extracted up to 2000 Hz—significantly above the standard's cut-off frequency—to ensure modal mass participation in the subsequent superposition steps with a ratio of effective mass to total mass of over 0.9.

The following tests were simulated using FEA tools on both the stator and rotor assemblies:

- Functional Random Vibration Test
- Long-Life Endurance Test
- Shock Test

The first two were conducted using random vibration profiles defined by power spectral density (PSD) curves using the modal superposition method. These excitation signals are analogous in both simulations, exciting the sample in all directions simultaneously from 10 to 500 Hz. The difference between the two tests lies in the vibration intensity for the vertical, transverse, and longitudinal excitations as shown in Table 6. The higher intensity in the second test represents the

Table 6. Equivalent RMS accelerations FOR random vibration excitations according to EN 61373:2010.

Direction	Functional random vibration	Long-Life endurance
Vertical	*3.88 g*	*14.69 g*
Transverse	*3.47 g*	*13.16 g*
Longitudinal	*1.73 g*	*6.56 g*

effects of ageing in the materials. A conservative damping ratio of 2%, typical of standard bolted assemblies, was applied, ensuring the design's reliability even under unfavourable conditions. All simulation results were evaluated using a 3σ (99.7%) statistical level, in accordance with the standard's prescribed methodology for random vibrations and ensuring structural integrity under the most restrictive scenario.

The shock test was simulated using a transient dynamic model in the time domain, applying half-sine acceleration pulses of 1000 m/s^2 (100 g) lasting 6 ms, independently in all three axes (vertical, longitudinal and transverse) with a time step of 0.5 ms. Unlike a static equivalent analysis, this time-domain approach captures the inertial effects and the dynamic amplification of the internal components. This is particularly critical for the permanent magnets and the cantilevered stator overhangs, which may experience local acceleration peaks higher than the input pulse due to their own flexibility. The acceptance criterion mandated a safety factor greater than 1 against yielding, ensuring that even under these extreme, rare events, the motor components suffer no permanent deformation and maintain their geometric tolerances for continued operation, with particular attention to the air gap.

The results discussed below focus on the mechanical response of the motor under shock and vibration conditions, emphasising the integrity of structural and sealing components under dynamic loading.

The most critical behaviour was found in the stator assembly due to its cantilevered mounting. To improve stiffness without compromising mass, 7075 aluminium was selected for the housing and axlebox interface components, contributing to higher power density and resistance to both static and dynamic loads.

The most critical stress distribution was observed during the long-life vibration test. In this case, the peak stress reached 261 MPa, localised at the motor's mounting interface with the axlebox (see Figure 12). This result, while representing the worst-case scenario across all simulated conditions, remains well below the yield strength of 7075 aluminium, providing a safety margin greater than 1.5 (excluding the local peak stress due to the stress concentration at the bolted interface) and confirming the structural integrity of the design under extended vibration exposure.

The 1.3 mm physical air gap proved sufficient to prevent rotor-stator contact under the worst-case displacement scenario. The most critical test in terms of displacement is the transverse shock, with a total displacement of 0.49 mm providing a gap-to-displacement ratio of 2.65 (see Figure 13).

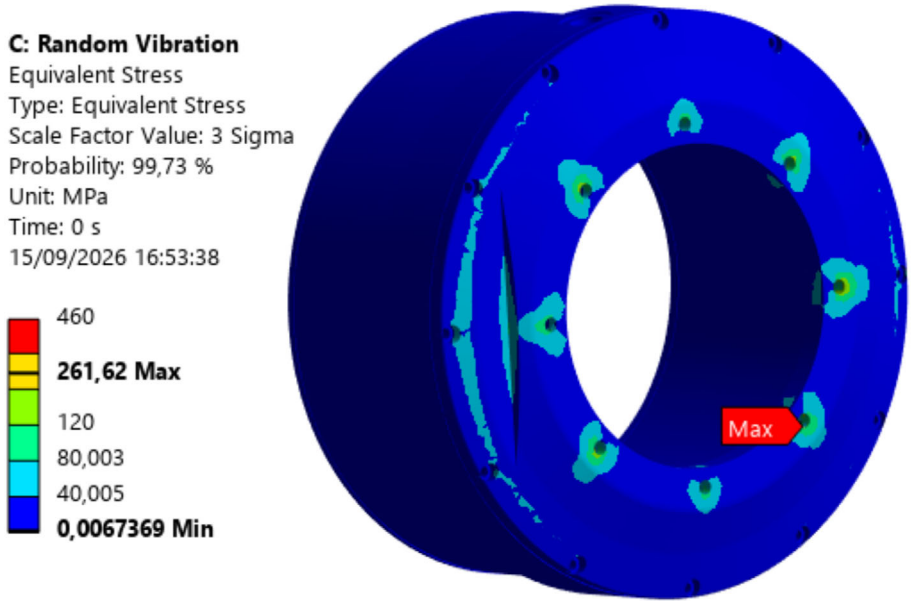


Figure 12. Equivalent von Mises stress map under dynamic loads (long-life test).

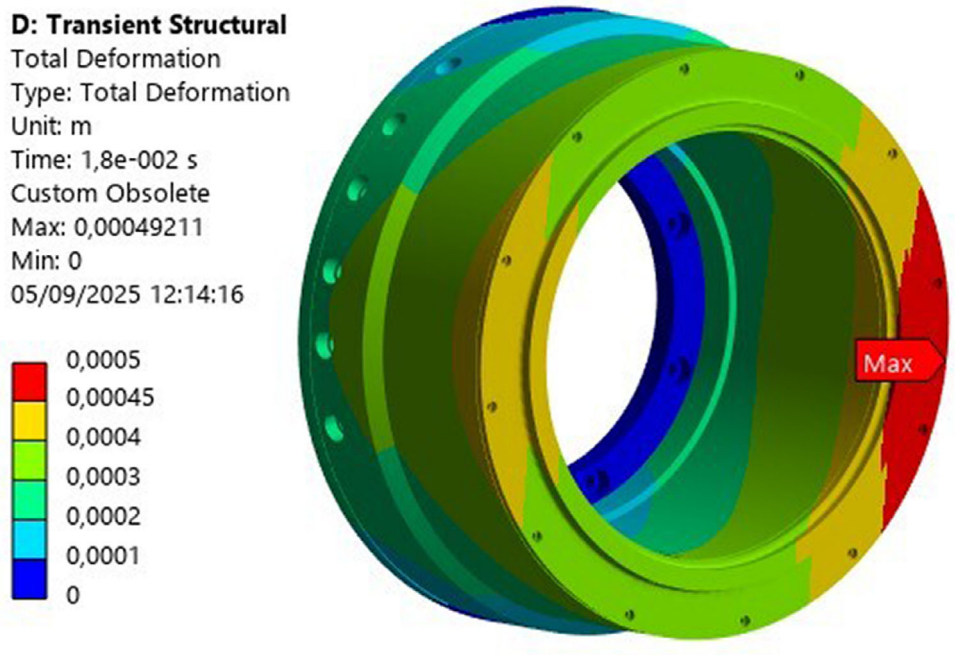


Figure 13. **Displacement map under dynamic loads (transverse shock).**

Table 7. **Final detailed-design mass breakdown.**

Component group	Mass [kg]
Rotor active parts (laminations and magnets)	*29.70*
Rotor sleeve and pressure plates	*3.80*
Stator active parts (laminations and winding)	*33.27*
Housing, cooling jacket, endplates and seals	*14.00*
Axlebox attachment	*3.34*
Cooling oil	*2.79*
Total	**86.90**

3.3 Final assembly mass and power density

The final detailed-design mass breakdown is summarised in Table 7. The complete motor assembly has a calculated mass of 86.90 kg, including 2.79 kg of cooling oil. The rotor and stationary assemblies account for 33.50 kg and 53.40 kg, respectively.

At the predicted continuous output of 275 kW, the complete-assembly power density is 3.16 kW/kg. The active electromagnetic parts weigh 62.97 kg, corresponding to 4.37 kW/kg. The final active-part mass is lower than the corresponding estimate used in the preliminary parametric comparison.

4. Comparison with state-of-the-art powertrains

4.1 Duty-cycle benchmarking against the reference induction-motor powertrain

To quantify the benefits of the proposed direct-drive PMSM, a comparative study was conducted against a traditional induction motor coupled to a gearbox. The comparison focuses on three key indicators: power density, system efficiency and life-cycle operating cost over the target duty cycle shown in Figure 14 and defined in the EN 50591 standard.[31] The comparison assumes an annual mileage of 400,000 km as specified by the train manufacturer. It is important to note a conservative constraint in this analysis regarding the operating speed. While the proposed direct-drive PMSM is optimised for a nominal speed of 360 km/h, the standard EN 50591 duty cycle is currently limited to a maximum of 300 km/h. Consequently, the simulation does not fully capture the motor's efficiency advantage in the ultra-high-speed

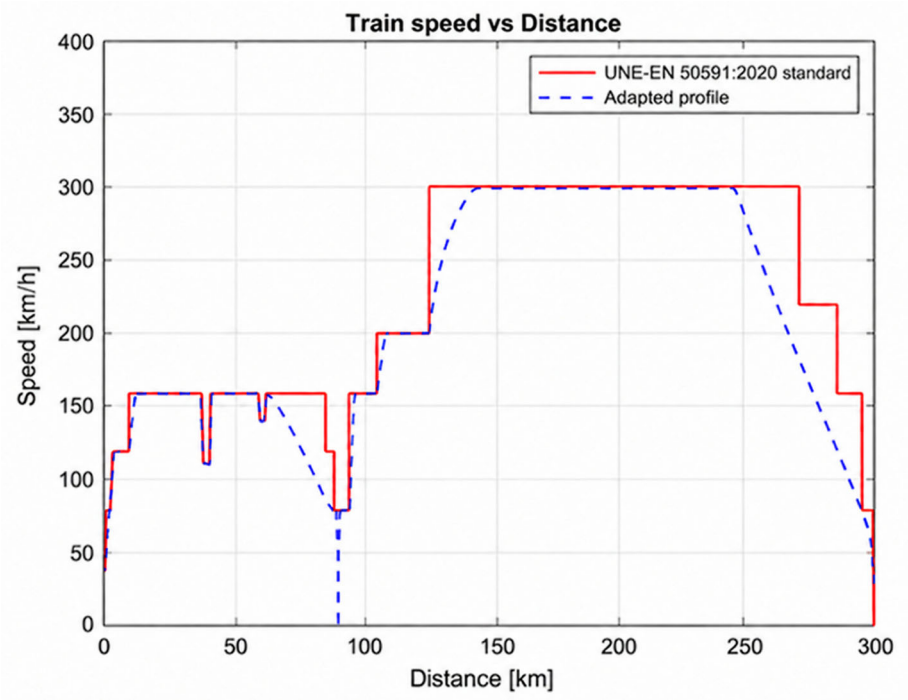


Figure 14. Reference and adapted speed profiles used for the 300 km duty-cycle assessment.

region for which it was designed. It is expected that as standards evolve to reflect higher commercial speeds, the relative performance of the proposed solution would further improve.

To evaluate the impact of the proposed motor on the train's overall energy footprint, three distinct traction configurations were simulated:

- **Baseline Scenario (Induction Motor + Gearbox):** This represents the current state-of-the-art traction chain provided by the manufacturer. The simulation accounts for the inherent limitations of induction technology, specifically the efficiency drop-off at partial loads and high speeds, alongside the mechanical losses introduced by the gearbox. While the system achieves a peak nominal efficiency of 92.92%, the cycle-weighted efficiency drops to 88.27%. This discrepancy highlights the difficulty of induction motors in maintaining optimal performance across the wide torque-speed envelope required by high-speed rail.

- **High-Speed Boost Strategy:** In this hybrid configuration, the proposed PMSM is added to the existing traction chain but operates solely as a "booster" at speeds exceeding 150 km/h. By offloading the induction motor in the high-speed region, where its efficiency typically degrades, the PMSM (nominal efficiency 95.54%) improves the combined system performance. However, since the PMSM is idle during acceleration below 150 km/h and low-speed operation, its impact is localised. The combined system achieves a cycle-weighted efficiency of 92.4%, with the PMSM averaging 95.3% during its active periods.

- **Load-Sharing Strategy (Full Range):** In this scenario, the PMSM operates continuously, independently of vehicle speed. The control strategy prioritises the PMSM to handle the base load, leveraging its superior partial-load efficiency to minimise losses, while the induction motor provides torque as needed. This approach maximises the utilisation of the high-efficiency direct-drive unit (average cycle efficiency of 94.61%), allowing the induction motor to operate closer to its nominal point. Consequently, the combined system efficiency reaches its peak at 93.73%.

The economic and environmental assessment focuses on the operational expenditure and CO2-equivalent emissions over the defined life cycle. The KPIs selected are the total operating cost and the total tons of CO_2 emitted during the life cycle of the motor, calculated under the following boundary conditions: an energy cost of 80 USD/MWh, a projected 2050

Table 8. Results of the economic and environmental benchmarking.

	Baseline scenario	High-Speed boost strategy	Load-Sharing Strategy
Life-cycle energy cost [million $]	*30.45*	*29.09*	*28.68*
Emissions [ton CO_2]	*3,013*	*2,879*	*2,837*
Reduction in KPIs relative to baseline [%]	*0.00*	*4.46*	*5.82*

Table 9. Comparison of the proposed motor with the PINTA3/MK5 demonstrator.

Parameter	PINTA3/MK5	Proposed design
Continuous power [kW]	350	275
Envelope diameter [mm]	660	430
Axial length [mm]	211	230
Envelope volume [L]	72.19	33.40
Power density [kW/L]	4.85	8.23
Existing disc-brake hardware at motorised wheel	Not retained	Retained by design
Validation status	Tested experimentally	Numerical assessment

energy mix for Spain (95% renewable penetration), a carbon tax of 250 USD/ton CO_2 and 0.16 ton CO2/MWh of non-renewable energy.[42,43,44,45]

The results of the assessment are described in Table 8. This benchmarking confirms that integrating a high-efficiency direct-drive PMSM not only improves energy conversion but also translates into substantial economic savings and a reduction in emissions, even under standard cycles that do not fully exploit the motor's high-speed capabilities. It is worth noting that this comparison isolates the operational gains of retrofitting or adding the PMSM to the existing architecture. In a new train design scenario, the economic case would be further strengthened by the elimination of the gearbox, as the capital expenditure savings from removing the transmission and the reduction in maintenance operations would likely offset the higher material cost of the permanent magnets.

4.2 Design comparison with the PINTA3/MK5 demonstrator

The previously mentioned PINTA3/MK5 demonstrator provides a relevant reference for assessing the compactness and integration requirements of the proposed motor. Table 9 compares both designs using an envelope-based volumetric power density, defined as continuous mechanical power divided by the bounding-cylinder volume. The MK5 yields 4.85 kW/L, compared with 8.23 kW/L for the proposed design. Thus, the proposed motor provides 78.6% of the reported MK5 continuous power within 46.3% of its cylindrical-envelope volume, corresponding to a 69.8% increase in envelope-based volumetric power density. This improvement is achieved under the additional integration constraint of retaining the existing disc-brake hardware, whereas the published MK5 motor-on-wheel configuration omitted the brake disc at the motorised wheel and considered braking compensation elsewhere in the train.[26,27]

5. Conclusions

This work presents the complete design process and multiphysics simulation of a high-performance, direct-drive permanent magnet synchronous motor (PMSM) for axle-mounted railway applications. Developed to provide additional traction in high-speed trains without modifying the existing bogie architecture, the proposed solution achieves a rated power of 275 kW with a nominal efficiency of 95.54%, all within a compact envelope offering power densities of 8.23 kW/L and 3.16 kW/kg for the final assembly, with a calculated assembly mass of 86.90 kg, including cooling oil. Its performance under both nominal and fault conditions supports its application as a next-generation direct-drive system for railway propulsion, reducing CO2 emissions and operating costs by between 4.46% and 5.82% when compared to current state-of-the-art railway traction solutions.

Structural simulation was carried out under both static and dynamic loading scenarios according to EN 13749 and EN 61373 standards. The stator and rotor demonstrated compliant stress and displacement behaviour under worst-case mechanical loads, including shock and vibration simulations.

The next stage of this work will focus on the experimental validation of the proposed motor through prototype testing, with particular emphasis on electromagnetic performance, thermal behaviour and mechanical integrity.

Ethics and consent

Ethical approval and consent were not required.

Declaration of AI-assisted preparation

During manuscript preparation, the authors used ChatGPT and Codex (OpenAI) to improve English grammar, wording and readability. OpenAI image-generation tools were also used to assist in preparing descriptive schematics based on CAD views and sketches supplied by the authors. These schematics are explanatory illustrations and do not represent simulation outputs or experimental measurements. The authors reviewed and corrected the AI-assisted content and take full responsibility for the accuracy and integrity of the manuscript and supporting material.

Data and software availability

Underlying data

Selected non-confidential design inputs, simulation conditions, processed numerical results and derived calculations are provided in the supporting Excel dataset deposited with Zenodo Supporting data for Design of a Direct-Drive Axle-Mounted Traction Motor for Boosting High-Speed Trains: https://doi.org/10.5281/zenodo.22829928.[46]

The Excel workbook covers the motor configuration, electromagnetic and thermal assessments, structural analyses, component masses and power densities, topology refinement, multiobjective optimisation settings and duty-cycle benchmarking. Data origins and relevant assumptions are identified in the corresponding worksheets.

Detailed CAD geometry, manufacturing and electrical-connection details, proprietary simulation-model definitions and individual optimisation-candidate geometries are not publicly disclosed because they contain industrial design information subject to confidentiality obligations and intellectual-property protection. The shared workbook documents the disclosed inputs and results but does not constitute a complete model archive for independently rerunning all simulations.

Data are available under the terms of the Creative Commons Attribution 4.0 International license (CC-BY 4.0).

Software availability

The design workflow used commercial simulation packages together with proprietary implementations of multiobjective differential evolution and topology optimisation. The proprietary source code is subject to institutional confidentiality restrictions and is not publicly available.

References

1. Brenna M, *et al.*: **A review on energy efficiency in three transportation sectors: Railways, electrical vehicles and marine.** *Energies (Basel).* May 2020; **13**(9): Art. no. 2378. **Publisher Full Text**
2. Ronanki D, Singh SA, Williamson SS: **Comprehensive Topological Overview of Rolling Stock Architectures and Recent Trends in Electric Railway Traction Systems.** *IEEE Transactions on Transportation Electrification.* Sep. 2017; **3**(3): 724–738. **Publisher Full Text**
3. Paul S, Han PW, Chang J, *et al.*: **State-of-the-art review of railway traction motors for distributed traction considering South Korean high-speed railway.** *Energy Rep.* Nov. 2022; **8**: 14623–14642. **Publisher Full Text**
4. Alstom SA:Accessed: Mar. 06, 2025. **Reference Source**
5. Bombardier Inc:Accessed: Mar. 06, 2025. **Reference Source**
6. SNCF:Accessed: Mar. 06, 2025. **Reference Source**
7. Eurostar:Accessed: Mar. 06, 2025. **Reference Source**
8. Cai S, Kirtley JL, Lee CHT: **Critical Review of Direct-Drive Electrical Machine Systems for Electric and Hybrid Electric Vehicles.** *IEEE Transactions on Energy Conversion.* Dec. 2022; **37**(4): 2657–2668. **Publisher Full Text**
9. Ma G, Sun Z, Xu S, *et al.*: **Review on permanent magnet direct drive technology of railway vehicles.** *Journal of Traffic and Transportation Engineering.* 2021; **21**(1): 217–232. **Publisher Full Text**
10. Deepak K, Frikha MA, Benômar Y, *et al.*: **In-Wheel Motor Drive Systems for Electric Vehicles: State of the Art, Challenges, and Future Trends.** *Energies (Basel).* Mar. 2023; **16**(7): 3121. **Publisher Full Text**
11. Biček M, Kunc R, Zupan S: **Mechanical Impact on In-Wheel Motor's Performance.** *J. Mech.* Oct. 2017; **33**(5): 607–618. **Publisher Full Text**
12. Biček M, Connes R, Omerović S, *et al.*: **The bearing stiffness effect on in-wheel motors.** *Sustainability (Switzerland).* May 2020;

12(10): 4070.
Publisher Full Text

13. Nategh S, *et al.*: **A Review on Different Aspects of Traction Motor Design for Railway Applications.** *IEEE Trans. Ind. Appl.* May 2020; **56**(3): 2148–2157.
Publisher Full Text

14. Caballero González D: *Cálculo y diseño de motores eléctricos de tracción ferroviaria. Comparativa de máquinas de inducción y de imanes permanentes.* Tecnun, San Sebastian: Universidad de Navarra; 2016.

15. Kondo M: **Application of Permanent Magnet Synchronous Motor to Driving Railway Vehicles.** *Railway Technology Avalanche.* 2003; **1**: 6.

16. Demmelmayr F, Troyer M, Schroedl M; **Advantages of PM-machines Compared to Induction Machines in Terms of Efficiency and Sensorless Control in Traction Applications.** *IECON 2011-37th Annual Conference on IEE Industrial Electronics Society.* Melbourne, VIC, Australia: IEEE; 2011; pp. 2762–2768.
Publisher Full Text

17. Gundogdu T, Zhu ZQ, Chan CC: **Comparative Study of Permanent Magnet, Conventional, and Advanced Induction Machines for Traction Applications.** *World Electr. Veh. J.* Aug. 2022; **13**(8): 137.
Publisher Full Text

18. Rabinovich YM, Sergeev VV, Maystrenko AD, *et al.*: **Physical and mechanical properties of sintered Nd-Fe-B type permanent magnets.** *Intermetallics (Barking).* Jan. 1996; **4**(8): 641–645.
Publisher Full Text

19. Bao XQ, *et al.*: **Regulating fracture behaviors and mechanical properties of sintered Nd–Fe–B magnet by reconstructing grain boundaries.** *Rare Metals.* May 2025; **44**: 3351–3361.
Publisher Full Text

20. Liu W, Wu J: **Mechanical properties and fracture mechanism study of sintered Nd-Fe-B alloy.** *J. Alloys Compd.* Jun. 2008; **458**(1–2): 292–296.
Publisher Full Text

21. Wang HJ, Guo ZH, Li AH, *et al.*: **Anisotropy of mechanical properties in sintered Nd-Fe-B magnets.** *J. Magn. Magn. Mater.* 2006; **303**(2 SPEC. ISS): e392–e395.
Publisher Full Text

22. Tang W, *et al.*: **Magnetic and mechanical properties of grain-refined Dy-free Nd-Fe-B sintered magnets.** *J. Magn. Magn. Mater.* Mar. 2021; **521**: 167533.
Publisher Full Text

23. Hoffmann J, Canders WR, Henke M: **Impact of current density and cooling on the weight balance of electrical propulsion drives for aviation.** *Energies (Basel).* Nov. 2020; **13**(22): 6149.
Publisher Full Text

24. Canders WR, Hoffmann J, Henke M: **Cooling technologies for high power density electrical machines for aviation applications.** *Energies (Basel).* Dec. 2019; **12**(23): 4579.
Publisher Full Text

25. Paredes Puente J: *Design and analysis of a novel stator oil-flooded cooling system for aircraft electrical machines with hairpin windings.* Tecnun, San Sebastian: Universidad de Navarra; 2022.

26. Europe's Rail Joint Undertaking: **Towards more efficient, Silicon Carbide-based traction systems.**
Reference Source

27. de la Guerra E: **Development of a new traction system for independent rotating wheel bogie.** *11th World Congress on High-Speed Rail.* Morocco: Marrakech; 2023.
Reference Source

28. Talgo:Accessed: Mar. 09, 2026.
Reference Source

29. Talgo Avril:Accessed: Mar. 09, 2026.
Reference Source

30. Feng Xue ACS, Graves RJ: **Multi-objective differential evolution - algorithm, convergence analysis, and applications.** *2005 IEEE Congress on Evolutionary Computation.* IEEE; 2005; pp. 743–750.
Publisher Full Text

31. European Committee for Electrotechnical Standardization: **Railway Applications - Rolling Stock - Specification and verification of energy consumption.** *EN 50591:2020.* 2020.

32. Lucchini F, Torchio R, Cirimele V, *et al.*: **Topology Optimization for Electromagnetics: A Survey.** *IEEE Access.* 2022; **10**: 98593–98611.
Publisher Full Text

33. Altair Engineering Inc: **Altair Flux 2D.**Accessed: Mar. 04, 2026.
Reference Source

34. Ansys Inc: **Ansys Fluent.**Accessed: Mar. 04, 2026.
Reference Source

35. Morales-Ramiro J, *et al.*: **Accionamiento Directo de Motor Eléctrico para Ruedas de Vehículos Ferroviarios.** *PCT/ES2025/070183.* Apr. 07, 2025.

36. Ansys Inc: **Ansys Mechanical.**Accessed: Mar. 05, 2026.
Reference Source

37. Budynas RG, Nisbett JK: *Shigley's Mechanical Engineering Design.* McGraw-Hill Education;Eleventh edition 2020.

38. European Committee for Standardization: **Railway applications - Wheelsets and bogies - Method of specifying the structural requirements of bogie frames.** *EN 13749:2011.* 2011.

39. Verein Deutscher Ingenieure: **Systematic calculation of highly stressed bolted joints - Joints with one cylindrical bolt.** *VDI 2230 Part 1:2014.* 2014.

40. European Committee for Electrotechnical Standardization: **Electric traction. Rotating electrical machines for rail and road vehicles. Part 2: Electronic converter-fed alternating current motors.** *EN 60349-2:2010.* 2010

41. European Committee for Electrotechnical Standardization: **Railway applications-Rolling stock equipment-Shock and vibration tests.** *EN 61373:2010.* 2010.

42. International Energy Agency: **World Energy Outlook 2024.** 2024. Accessed: Sep. 24, 2026.
Reference Source

43. International Energy Agency: **Achieving Net Zero Electricity Sectors in G7 Members.** 2021. Accessed: Sep. 24, 2026.
Reference Source

44. eurostat: **Renewable energy statistics.**Accessed: Mar. 26, 2026.
Reference Source

45. Petrovich B: **European electricity prices and costs.** *Ember-Energy (daily update).*Accessed: Mar. 26, 2026.
Reference Source

46. Morales-Ramiro J, Satrústegui M, Landa Ansa E, *et al.*: "Supporting data for Design of a Direct-Drive Axle-Mounted Traction Motor for Boosting High-Speed Trains," version 1.0. dataset. *Zenodo.* 2026.
Publisher Full Text